A treatise on InSAR geometry and 3D displacement estimation

Wietske S. Brouwer and Ramon F. Hanssen, *Senior Member, IEEE*

***Abstract*—It is well known that InSAR phase observations are only sensitive to the projection of the 3D displacement vector onto the radar line-of-sight (LoS) direction. We require at least three LoS observations to uniquely estimate the three displacement components, and the system of equations needs to have a full rank coefficient matrix. Unfortunately, in many practical situations, only two LoS observations are available at most (i.e., ascending and descending), resulting in an underdetermined system with an infinite amount of possible solutions. Yet, this has not prevented many authors from performing LoS decompositions that are fundamentally flawed. Starting with a mathematical framework based on linear algebra, we introduce the concept of the null line, the direction in which no displacements can be observed, and identify the strict criteria to perform decompositions and projections. We propose using a null-line aligned (NLA) reference frame, which results in bias-free estimates. Based on a literature survey, we identify the most common flaws in handling 3D InSAR geometry, and develop a taxonomy to label different classes of fallacies. This work results in recommendations for a more optimal and uniform handling of InSAR geometry, in terms of claims and results.**

***Index Terms*—InSAR, surface displacements, line-of-sight, decomposition, null line, solution space**

I. Introduction

IT is well known that InSAR phase observations are only sensitive to the projection of the 3D displacement vector onto the radar line-of-sight (LoS) direction, along a plane orthogonal to the LoS [1]. This projection, d_{LoS}, in a Cartesian east, north, up (ENU) coordinate system is described by

$$d_{\text{LoS}} = P_{\text{LoS}^\perp}\, d_{\text{ENU}}, \tag{1}$$

where $P_{\text{LoS}^\perp} = [\sin\theta \sin\alpha_d, \sin\theta \cos\alpha_d, \cos\theta]$ is the orthogonal projector onto the line of sight, $d_{\text{ENU}} = [d_e, d_n, d_u]^T$ is the 3D displacement vector in east, north, and up direction, respectively, θ is the incidence angle towards the radar, and α_d is the azimuth of the zero-Doppler plane at the position of the target, in the direction towards the satellite, see Fig. 1. In the early years of InSAR, one viewing geometry was used for estimating displacements [2], [3], [4]. However, the possibility to combine ascending and descending orbits imaging the same area of interest triggered attempts to estimate the 3D displacement vectors [5], [6], [7], [8]. Evidently, to estimate the full 3D displacement vector, one would need three independent viewing geometries, using three different $P_{\text{LoS}^\perp}$ projectors forming a full rank matrix with a low condition number [9]. Yet, while the near-polar orbits of contemporary SAR missions cause an imaging geometry that differs significantly between ascending and descending orbits, it does not for adjacent tracks [6], [10]. As a result, the sensitivity is rather unbalanced for the three Cartesian directions [1]. Moreover, in many practical situations only two LoS observation geometries are available, i.e., ascending and descending, resulting in an underdetermined system with an infinite amount of possible solutions. While this rank deficiency is rather trivial, a systematic survey of InSAR literature reveals that approaches to address it often have either mathematical or semantic flaws, as we will discuss in Sec. V. The impact of these flaws causes quantitative errors in the reported studies and mismatches in comparative studies with other geodetic techniques, leading to a lack of trust in the technology by end-users and problems in the interpretation of the results.

The root cause of these flawed or erroneous statements and results seems to originate from a rather lax mathematical definition of the problem, negligence of the geographic location of the region of interest, and sometimes its definition from the satellite's rather than the target's perspective. Moreover, we observe a rather indiscriminate handling of the concepts

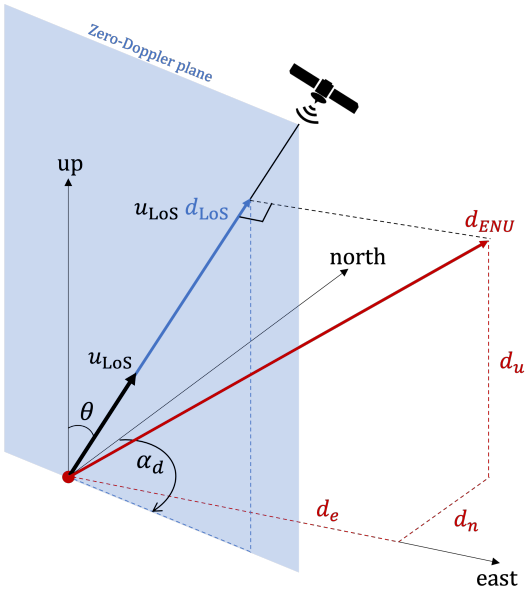

Fig. 1: Schematic overview of the projection of the displacement vector d_{ENU} onto the LoS direction of a satellite in a descending orbit. The LoS direction of the satellite can be described with two angles: the incidence angle θ and the azimuth of the zero-Doppler plane α_d. Those angles are described at the position of the target.

W.S. Brouwer and R.F. Hanssen are with the Department of Geoscience and Remote Sensing, Delft University of Technology, Delft, 2628 CN, The Netherlands (email: w.s.brouwer@tudelft.nl, r.f.hanssen@tudelft.nl).

projection and *decomposition*, and a lack of explicitly stated (and often unsubstantiated) assumptions that serve as boundary conditions.

In this study, we provide an overarching and rigid mathematical framework rooted in linear algebra, building on previous work by [1], [6], [7] and [8] (Sec. II), explicitly state the conditions for a successful inversion (Sec. III), and introduce of the concept of the null line (Sec. IV). Using these concepts, we analyze and classify the different classes of fallacies related to the InSAR geometry problem encountered in literature in Sec. V and provide recommendations for InSAR product generation and interpretation in Sec. VI.

II. Theory

To solve for the full 3D displacement vector, several conditions (all necessary but individually not sufficient) need to be satisfied. Therefore, we first review the relevant InSAR geometry and the forward model in Sec. II-A and II-B, respectively.

A. The viewing geometry

The estimated relative displacements resulting from InSAR parameter estimation are projections onto the line-of-sight (LoS) direction. These need to be defined from the perspective of the target, since this is the object that is in motion. The LoS direction depends on the viewing geometry towards the satellite, that can be described using two angles: the azimuth of the zero-Doppler plane at the Earth's surface, α_d, and the incidence angle, θ, see Fig. 1.

1) Azimuth of the zero-Doppler plane: Most SAR satellites operate from retrograde sun-synchronous near-polar orbits. While the orbital plane of the satellite has a fixed inclination, both the ascending and descending track have a time-varying orbital heading α_h, which is the angle between the velocity vector of the satellite and the geometrical north. For most SAR satellites, the observations are taken at zero-Doppler [1]. We can therefore define the zero-Doppler plane (ZDP), which is the plane perpendicular to the heading of the satellite.

The heading, α_h, and consequently the orientation of the ZDP, in a satellite-centered coordinate frame, are different from the direction of the velocity vector and the azimuth of the ZDP, α_d, in a target-centered coordinate frame, i.e., on the Earth's surface, see Fig. 2. This effect is caused by the side-looking geometry of the SAR and the non-parallel nature (convergence) of the Earth's meridians. Additionally, the azimuth of the zero-Doppler plane is range dependent. These effects should be taken into account when computing the viewing geometry since the difference can be significant, especially at higher latitudes, e.g., the projector $P_{\text{LoS}^\perp}$ should be defined by α_d rather than by α_h.

2) Incidence angle: The incidence angle, θ, refers to the nominal (ellipsoidal) incidence angle, i.e., the angle between the normal vector on the local ellipsoid, at the position of the target, and the line of sight towards the satellite in the ZDP. The incidence angle should not be confused with the satellite look angle θ_l, which is the angle between the LoS direction and the nadir of the satellite sensor, see Fig. 3. Moreover,

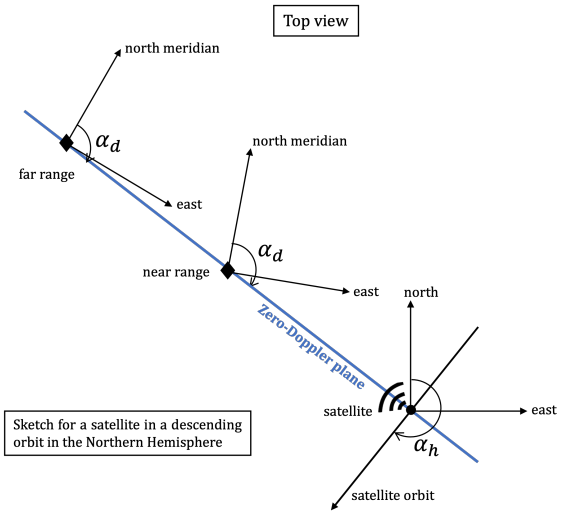

Fig. 2: Two targets on Earth (black diamonds) are observed from a satellite (black dot) in a descending orbit in the Northern Hemisphere. The velocity vector of the satellite has azimuth angle α_h with respect to the geographical north. Due to the meridian convergence, the north direction at the Earth's surface at near range (nr) differs from the north direction at far range (fr). Therefore, the orientation of the zero-Doppler plane (in blue) differs, depending on the target position, i.e., $\alpha_{d,\text{nr}} \neq \alpha_{d,\text{fr}}$.

the nominal incidence angle varies with the range direction resulting in different incidence angles for different targets (pixels) within the same image. For example, the incidence angle for Sentinel-1 Interferometric Wide (IW) swath varies between 29° and 46° [11].

As both the incidence angle and azimuth of the ZDP are range dependent, they are correlated. Due the meridian convergence, the orientation of the target-centered coordinate system with respect to the satellite-centered coordinate system differs from near to far range, see Fig. 2. Therefore, α_d is range dependent, i.e., $\alpha_{d,\text{nr}} \neq \alpha_{d,\text{fr}}$ where $\alpha_{d,\text{nr}}$ is the azimuth of the ZDP at near range and $\alpha_{d,\text{fr}}$ the azimuth of the ZDP at far range. Since the incidence angle also varies with range, both angles are correlated. The interdependence between θ and α_d is visualized in Fig. 4. Using the Delft Radar Modelling and performance Analysis (DRaMA) toolbox [12], we estimated the viewing geometries of all available Sentinel-1 acquisitions, and visualized θ and α_d for all available ascending (top) and descending (bottom) acquisitions for locations at sea level with a varying latitude and an arbitrary longitude, here 40°E. High-latitude locations on Earth are observed in multiple swaths, indicated by the dots.

B. Forward model

The displacement d_{LoS} of a target observed from a satellite is the orthogonal projection of d_{ENU} onto the LoS direction, see Eq. (1). We refer to this as a *forced* projection, as it is an implicit autonomous operation. As Eq. (1) represents the

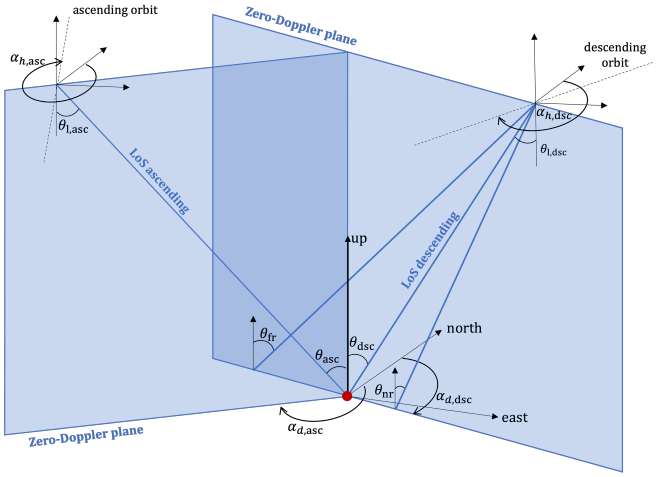

Fig. 3: Schematic overview of the viewing geometry. The heading angles $\alpha_{h,\text{asc}}$ and $\alpha_{h,\text{dsc}}$ are the azimuth angles of the velocity vectors of the satellites with respect to the geometrical north. α_d is the azimuth of the zero-Doppler plane, at the position of the target (red dot), in the direction towards the satellite. The incidence angle is the angle between the LoS vector and the local zenith and varies from near to far range, i.e. $\theta_{\text{fr}} > \theta_{\text{nr}}$.

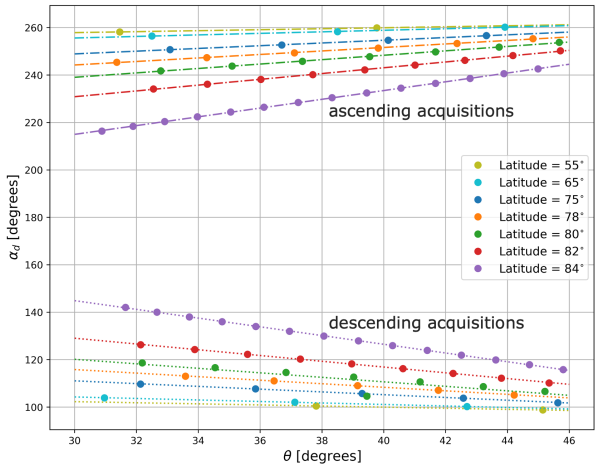

Fig. 4: For different latitudes, at an arbitrary longitude 40°E, the viewing geometries towards the visible Sentinel-1 swaths (circular marks) are shown. At the top, the positive correlation between α_d and θ for ascending acquisitions can be seen. For descending acquisitions (bottom) there is a negative correlation. It can also be seen that on average, α_d is lower at higher latitudes for ascending acquisitions and higher for descending acquisitions. Note that we show the correlation between θ and α_d for the Northern Hemisphere, for the Southern Hemisphere the correlation has an opposite sign.

displacement as a scalar, it requires a directional unit vector to specify its direction, i.e.,

$$d_{\text{LoS}}\,\mathrm{u}_{\text{LoS}} = P_{\text{LoS},\text{LoS}^\perp}\,d_{\text{ENU}} = P_{\text{LoS}^\perp} I_3\,d_{\text{ENU}}, \tag{2}$$

where u_{LoS} is the LoS unit vector, defined as

$$\mathrm{u}_{\text{LoS}} = \begin{bmatrix}\mathrm{u}_1\\ \mathrm{u}_2\\ \mathrm{u}_3\end{bmatrix} = \begin{bmatrix}\sin\theta\sin\alpha_d\\ \sin\theta\cos\alpha_d\\ \cos\theta\end{bmatrix}, \tag{3}$$

and the notation $P_{\text{LoS},\text{LoS}^\perp}$ refers to a projector *onto* the LoS, *along* a plane orthogonal to the LoS unit vector. The LoS unit vector has its origin at the target. Motion towards the satellite yields a decrease in slant range. Since d_{LoS} is the orthogonal projection of the 3D displacement vector onto the LoS direction, displacement vectors situated in the plane orthogonal to the LoS direction result in $d_{\text{LoS}} = 0$, i.e., the radar is not sensitive to displacements in that direction.

Given this geometry and forward model, we can now evaluate the inverse model to estimate the displacement parameters and focus on the necessary and sufficient conditions for this estimation.

III. Conditions for the Inverse Model

The LoS displacements itself are one-dimensional and may be difficult to interpret by end-users, who are mostly interested in the 'real' 3D displacements. This requires a *decomposition* of the LoS displacements, i.e., the inverse problem [13]. The functional relation of Eq. (1) is therefore extended to a full mathematical model

$$E\{\underbrace{\begin{bmatrix}\underline{d}^{(1)}_{\text{LoS}}\\ \underline{d}^{(2)}_{\text{LoS}}\\ \vdots\\ \underline{d}^{(m)}_{\text{LoS}}\end{bmatrix}}_{\underline{y}}\} = \underbrace{\begin{bmatrix}P^{(1)}_{\text{LoS}^\perp}\\ P^{(2)}_{\text{LoS}^\perp}\\ \vdots\\ P^{(m)}_{\text{LoS}^\perp}\end{bmatrix}}_{A}\underbrace{\begin{bmatrix}d_e\\ d_n\\ d_u\end{bmatrix}}_{x}, \text{ and} \tag{4}$$

$$D\{\underbrace{\begin{bmatrix}\underline{d}^{(1)}_{\text{LoS}}\\ \underline{d}^{(2)}_{\text{LoS}}\\ \vdots\\ \underline{d}^{(m)}_{\text{LoS}}\end{bmatrix}}_{\underline{y}}\} = \underbrace{\begin{bmatrix}Q_{\text{LoS},1} & 0 & \dots & 0\\ 0 & Q_{\text{LoS},2} & \dots & 0\\ \vdots & \vdots & \ddots & \vdots\\ 0 & 0 & \dots & Q_{\text{LoS},m}\end{bmatrix}}_{Q_{yy}}, \tag{5}$$

where vector $\underline{y}$ is the observation vector, composed of vectors $\underline{d}^{(1)}_{\text{LoS}}$ until $\underline{d}^{(m)}_{\text{LoS}}$, which are m sets of LoS displacement observations from scatterers within the same region of uniform motion (RUM, further elaborated on in Sec. III-B). The underline indicates the stochastic nature of the vector. Each vector $\underline{d}^{(i)}_{\text{LoS}}$ represents an independent viewing geometry, i.e., the set of all observation points (scatterers) observed from a particular satellite orbit, where the size of each set can be different since the number of available coherent scatterers within a RUM can differ. A 'set' refers to all observations from one viewing geometry. $E\{.\}$ expresses the expectation operator. $D\{.\}$ is the dispersion of the model, where $Q_{\text{LoS},i}$ is the variance-covariance matrix of an independent observation set. When $\underline{d}^{(i)}_{\text{LoS}}$ has size $p \times 1$, i.e., there are p scatterers within

the RUM for that particular viewing geometry, the size of $Q_{\text{LoS},i}$ is $p \times p$. It is a diagonal matrix with the variances of the LoS observations on the diagonal. The off-diagonal elements are equal to zero, since all observations represent different physical scatterers, i.e., with different reflective characteristics of the imaged objects, acquired at different times.

This system of observation equations can be solved with at least three sets of LoS observations, i.e. $\underline{d}^{(1)}_{\text{LoS}}$, $\underline{d}^{(2)}_{\text{LoS}}$ and $\underline{d}^{(3)}_{\text{LoS}}$, that are spatio-temporally coinciding and independent (STCI, further discussed in Sec. III-A). The row for the first set in the design matrix A is the projection of the 3D displacements onto the LoS vectors towards the first satellite position. We assume that for the observations within one set, the incidence angle θ and azimuth of the ZDP α_d are constant within the RUM.

When $m \geq 3$, the unknown displacement parameters in vector x can be estimated using direct inversion or Best Linear Unbiased Estimation (BLUE) [14], i.e.,

$$\underline{\hat{x}} = \begin{cases} A^{-1}\underline{y}, & \text{for } m = 3, \text{ and} \\ Q_{\hat{x}}A^T Q_{yy}^{-1}\underline{y} & \text{for } m > 3, \text{ with} \end{cases} \tag{6}$$

$$Q_{\hat{x}\hat{x}} = \begin{cases} A^{-1}Q_{yy}A^{-1}, & \text{for } m = 3, \text{ and} \\ (A^T Q_{yy}^{-1}A)^{-1} & \text{for } m > 3. \end{cases} \tag{7}$$

For a successful estimation of the unknown displacement parameters this approach needs to satisfy five conditions, which need to be explicitly stated. Below, we elaborate on the concepts STCI, RUM, datum, rank, and angular diversity.

A. Spatio-temporally coinciding independent (STCI) LoS observations

The mathematical expression of Eq. (6) is only valid if all LoS observation sets from different viewing geometries are unambiguously linked to the same physical displacement signal, x. In reality, this is almost never exactly the case, especially in the built environment. Therefore, using the concept of spatio-temporally coinciding independent (STCI) LoS observations, we mean that (i) the same scatterers, on (ii) an object that is not subject to internal deformation, are (iii) observed simultaneously by (iv) different viewing geometries. Thus, the following three conditions should be fulfilled:

1) the observations from the different viewing geometries should observe the same displacement signal or phenomenon.
2) This only works if the same (position on an) object would be measured by the different viewing geometries, while
3) the observations should be taken at the same moments in time (epochs).

While condition 1 is trivial, the second condition is related to the spatial part of the STCI LoS observations and is essential since scatters close to each other are not per definition stemming from the same object, e.g., consider a scatterer on the roof of a founded house and a scatterer nearby on the street, which both represent different deformation phenomena. Added to this, different objects (or parts of objects) can show different deformation phenomena [15], [16].

The third condition is related to the temporal part, which is required since by definition deformation phenomena change over time. Observations from the different acquisitions are never taken at the same moment. For rapidly changing deformation phenomena such as landslides or highly dynamic peat soils, it may be impossible to assume that observations from different epochs represent the same behavior. However, to be able to use observations from different viewing geometries, we need to assume that it is possible to interpolate the observations in time, which is only possible when the deformation phenomenon has a smooth behavior in time and is not rapidly changing between epochs.

B. Region of Uniform Motion

Obviously, the STCI condition described in Sec. III-A is hardly ever fulfilled for a single target. This would only be the case when point scatterers (PS) observed with one satellite would exactly match the PS of the other satellites, as e.g., with lamp posts [17], [18] or integrated geodetic reference stations (IGRS) [19]. Thus, more in general, the decomposition of the LoS observations should be based on the assumption that: *points that fall within one Region of Uniform Motion (RUM) behave according to the same deformation phenomenon.* So only after defining a RUM, and aligning the different data sets in time, it will be possible to decompose the LoS observations into the unknown displacements parameters. However, defining a RUM can be difficult, since it can easily contain scatterers which represent different deformation phenomena [20].

C. Datum connection

It is essential that the different LoS observations are referenced to the same reference point, since the LoS displacements are double-differences. Obviously, there are different reference points for the observations from different viewing geometries. Therefore, it is at least required that all reference points represent the same deformation phenomenon.

D. Full rank system

To unambiguously solve for the three unknown displacement components we require at least three sets of STCI observations from different viewing geometries, yielding a unique solution. Multiple observations from one set would not be sufficient since the observations within one RUM all belong to the same viewing geometry and the same deformation phenomena. This follows from analyzing the solution space for different cases. The solution space is the space that contains all possible solutions and is sometimes also called the null space. With only one LoS observation set, the solution space is a plane orthogonal to the LoS displacement vector that contains the end-point of the LoS vector. For a satellite in an ascending orbit, the solution space is the blue plane in Fig. 5, also called the null plane. All points located in the null plane are possible solutions to the inverse problem. The orientation of the null plane is completely defined by the LoS unit vector, u_{LoS}, see Eq. (3), which is normal to the null plane. The null plane

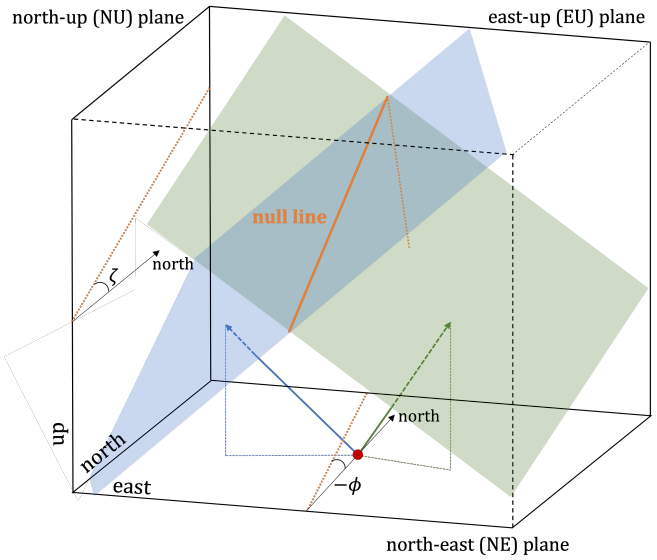

Fig. 5: When only one set of LoS observations is available, the solution space for the inverse problem is the plane orthogonal to the LoS direction (the blue plane for an ascending satellite and the green plane for a descending satellite). When two LoS observation sets are available, the two null planes intersect, where the intersection is the null line (shown in orange). All points located on the null line are a possible solution to the inverse problem. The null line is described by azimuth angle ϕ and elevation angle ζ.

further contains the end point of the LoS vector, see Eq. (2). The null plane is thus defined as

$$\mathrm{u}_1(x - d_{\mathrm{LoS,e}}) + \mathrm{u}_2(y - d_{\mathrm{LoS,n}}) + \mathrm{u}_3(z - d_{\mathrm{LoS,u}}) = 0, \quad (8)$$

where $d_{\mathrm{LoS,e}}$, $d_{\mathrm{LoS,n}}$ and $d_{\mathrm{LoS,u}}$ are the east, north and up components of the LoS vector respectively.

When two LoS observation sets are available, the null space reduces to a line, n, which we term the *null line*. This is visualized in Fig. 5, where the blue and green arrows are the LoS unit vectors corresponding to an ascending and a descending observation, the blue and green planes are the null planes, and the orange line is the null line (or null space) for the two observations. This null line contains the end-point of the unknown 3D displacement vector. However, the actual (correct) solution remains unknown since all points on the line are potential solutions to the underdetermined problem.

The orientation of the null line is an important metric for InSAR interpretation and is described by azimuth angle ϕ and elevation angle ζ. When the viewing geometry for both acquisitions is known, the orientation of the null line can be computed; the direction of the null line is given by the cross product of the two normal vectors of the null planes, which are the LoS unit vectors, and equals

$$n = \mathrm{u}_{\mathrm{LoS}}^{(1)} \times \mathrm{u}_{\mathrm{LoS}}^{(2)} = \begin{bmatrix} \sin\theta_1 \sin\alpha_{d,1} \\ \sin\theta_1 \cos\alpha_{d,1} \\ \cos\theta_1 \end{bmatrix} \times \begin{bmatrix} \sin\theta_2 \sin\alpha_{d,2} \\ \sin\theta_2 \cos\alpha_{d,2} \\ \cos\theta_2 \end{bmatrix} \quad (9)$$

where n is the vector indicating the direction of the null line, θ_1 and $\alpha_{d,1}$ correspond to the first viewing geometry and θ_2 and $\alpha_{d,2}$ to the second viewing geometry. From n it is possible to compute ϕ and ζ with

$$\phi = \tan^{-1}(\frac{n_1}{n_2}) \text{ and} \quad (10)$$

$$\zeta = \tan^{-1}(\frac{n_3}{\sqrt{n_1^2 + n_2^2}}), \quad (11)$$

where n_1, n_2, and n_3 are the east, north, and up component of n respectively. Displacement vectors in the direction of n have a projection into both LoS directions which is zero, i.e., both satellites are not sensitive for displacements into that direction.

To solve unambiguously for the 3D displacement vector, albeit with various degrees of precision, three or more sets of LoS observations are required. Only then, there is one unique point where the three null planes intersect.

The quality of the estimator $\hat{\underline{x}}$, see Eqs. (6) and (7), is found with the error propagation law as

$$Q_{\hat{x}} = (A^T Q_{yy}^{-1} A)^{-1} = \begin{bmatrix} \sigma_e^2 & \sigma_{en} & \sigma_{eu} \\ \sigma_{en} & \sigma_n^2 & \sigma_{nu} \\ \sigma_{eu} & \sigma_{nu} & \sigma_u^2 \end{bmatrix}. \quad (12)$$

The diagonal elements of $Q_{\hat{x}}$ give the variances for $\hat{d}_e$, $\hat{d}_n$, and $\hat{d}_u$ respectively. The requirement of working with three STCI LoS observation sets, stemming from the same RUM is a *necessary but insufficient* requirement. The three STCI LoS observation sets also need to have sufficiently different angular diversity to ensure full rank.

E. Angular diversity

Unfortunately, because almost all SAR satellites operate right-looking and orbit the Earth in near-polar retrograde orbits, they all have very similar viewing geometries, resulting in limited angular diversity between different SAR missions. The null line for each combination of any ascending and descending viewing geometry will be approximately in the same direction.

So even with LoS observations from three viewing geometries, the inverse problem solution is very unstable, i.e., a small difference in the LoS observations may lead to an enormous change in the estimated displacement components. As a result, the inverse problem is often ill-posed [13], even with observations from three viewing geometries, [6], [21], and A is close to rank deficient. This can be shown with the variance-covariance matrix, $Q_{\hat{x}\hat{x}}$, for the estimated displacement components. When simulating three different viewing geometries, consisting of two ascending acquisitions and one descending acquisition, it is possible to estimate the precision for the estimated displacement parameters as in Eq. (12). With ascending-1, ascending-2, and descending-1 as presented in Tab. I, simulating one scatterer per viewing geometry, and using $\sigma^2_{\mathrm{LoS}} = 1$ mm^2 for all three observations, we estimated $Q_{\hat{x}}$, see Fig. 6a. The diagonal of $Q_{\hat{x}}$ shows the variances of $\hat{d}_e, \hat{d}_n$ and $\hat{d}_u$. The precision (σ) with which we can estimate the north component is 39.7 mm, which is ∼40 times larger than the simulated σ's of the LoS observations. The precisions

TABLE I: Characteristics of the simulated viewing geometries

Geometry type	Incidence angle θ	Azimuth ZDP α_d
ascending-1	30°	260°
ascending-2	41°	261°
descending-1	44°	100°

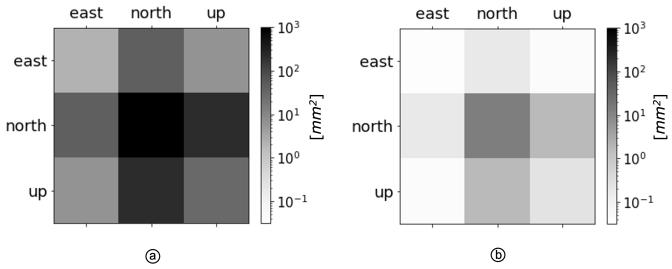

Fig. 6: The full variance-covariance matrix for the estimates for the three displacement components shown in a logarithmic scale. a) shows the situation where all observations are stemming from right-looking satellites, see Tab I. In b) there are two right looking satellites and one left looking satellite. It can be seen that there is a significant improvement on retrieving d_n, but also the other displacement components benefit from the addition of a left-looking radar acquisition.

for the east and up components are much better, i.e., 1.5 mm and 5.5 mm, respectively.

One solution to improve on retrieving d_n is to add a left-looking observation as suggested by [6] and [21]. In Fig. 6b, the variance-covariance matrix for a situation where the second ascending acquisition is changed to a left looking acquisition is shown. The precisions of the unknown parameters are now 0.3 mm, 4.5 mm, and 0.7 mm for d_e, d_n, and d_u respectively, which is an improvement for all components. However, the σ for d_n is still large, especially when we consider that the σ for the LoS observations was 1 mm.

IV. The null line

In many practical situations, the maximum number of sets of STCI LoS observations is two (one ascending and one descending), since almost all SAR satellites are operationally right-looking. This results in an underdetermined problem with an infinite number of possible solutions along the null line. With this rank deficiency it is impossible to provide a unique estimate for d_{ENU}. One of the possibilities is to take advantage of the orientation of the null space, by choosing a *null line aligned* (NLA) Cartesian coordinate system. This yields a plane orthogonal to the null line, and therefore the (forced) orthogonal projection of a displacement vector onto that plane will not influence (bias) the two in-plane components. Thus, the remaining two in-plane components can be uniquely and unbiasedly estimated. This option stresses the importance of the null line, in particular its orientation in three-dimensional space.

A. The orientation of the null line

We calculate the orientation of the null line at different locations on Earth for one ascending and one descending Sentinel-1 viewing geometry, using Eqs. (10) and (11), and No-DRaMA[1], see Figs. 7a and b. The values for ϕ and ζ, respectively the azimuth and elevation of the null line, are shown, cf. Fig. 5. This demonstrates that $\phi \approx 0°$ for the Northern Hemisphere, but that this is not always the case for the Southern Hemisphere. Moreover, everywhere on Earth the elevation angle $\zeta > 0°$.

At higher latitudes, different tracks overlap, enabling multiple ascending and descending viewing geometries per location. Therefore, Figs. 7a and b use the largest possible α_d per location, i.e., the largest asymmetry between the two viewing geometries.

To investigate whether $\phi = 0°$ can really be considered a 'rule of thumb' for the Northern Hemisphere for Sentinel-1, we compute ϕ and ζ for all possible combinations between ascending and descending acquisitions for latitudes varying between $-75°$ and $+85°$, at longitude 30°, see Figs. 7c and d. Typically for the Northern Hemisphere, all combinations result in $\phi = 0°$. Yet, for the higher southern latitudes, different combinations result in $\phi \neq 0°$. This would have practical impact for applications in Antarctica. Elevation angles ζ increase significantly when approaching the poles, affecting the Arctic, South America, South Africa, New Zealand, and the Antarctic.

B. Impact of the null line orientation

In many studies [23], [24], [25], [26], [27], [28], [29], [30], [31], [32], [33] it is postulated that with the current orbits and viewing geometry of SAR missions, there is no sensitivity for displacement components in the north direction, and that it is possible to simply 'remove' or 'disregard' d_n from the inverse problem. Effectively, this results in Eq. (4) changing to

$$E\{\underbrace{\begin{bmatrix} \underline{d}_{\text{LoS}}^{(1)} \\ \underline{d}_{\text{LoS}}^{(2)} \\ \vdots \\ \underline{d}_{\text{LoS}}^{(m)} \end{bmatrix}}_{y}\} = \underbrace{\begin{bmatrix} \sin\theta_1 & \sin\alpha_{d,1} & \cos\theta_1 \\ \sin\theta_2 & \sin\alpha_{d,2} & \cos\theta_2 \\ & \vdots & \\ \sin\theta_m & \sin\alpha_{d,m} & \cos\theta_m \end{bmatrix}}_{A} \underbrace{\begin{bmatrix} d_e \\ d_u \end{bmatrix}}_{x}. \quad (13)$$

Yet, this would only be a valid approach when the null line is indeed oriented in the north direction, i.e., if $\phi = 0° \wedge \zeta = 0°$. However, even while ϕ may be close to zero, $\zeta \neq 0$, and therefore this approach is flawed.

As can be seen in Fig. 6, the estimators for d_e, d_n and d_u are correlated. Therefore, simply 'removing' d_n from the inverse problem, will result in biased estimates for d_e and d_u, i.e.,

$$\begin{aligned} \hat{d}_e &= d_e + B_e \\ \hat{d}_u &= d_u + B_u, \end{aligned} \quad (14)$$

where B_e and B_u are the biases on the estimated east and up component, respectively.

Geometrically, by removing d_n from the decomposition equation, both LoS observations are implicitly projected onto

[1]No-DRaMA is a module of DRaMA [22] that computes the orientation of the null line for different satellite missions at different locations on Earth, it is available on gitlab.

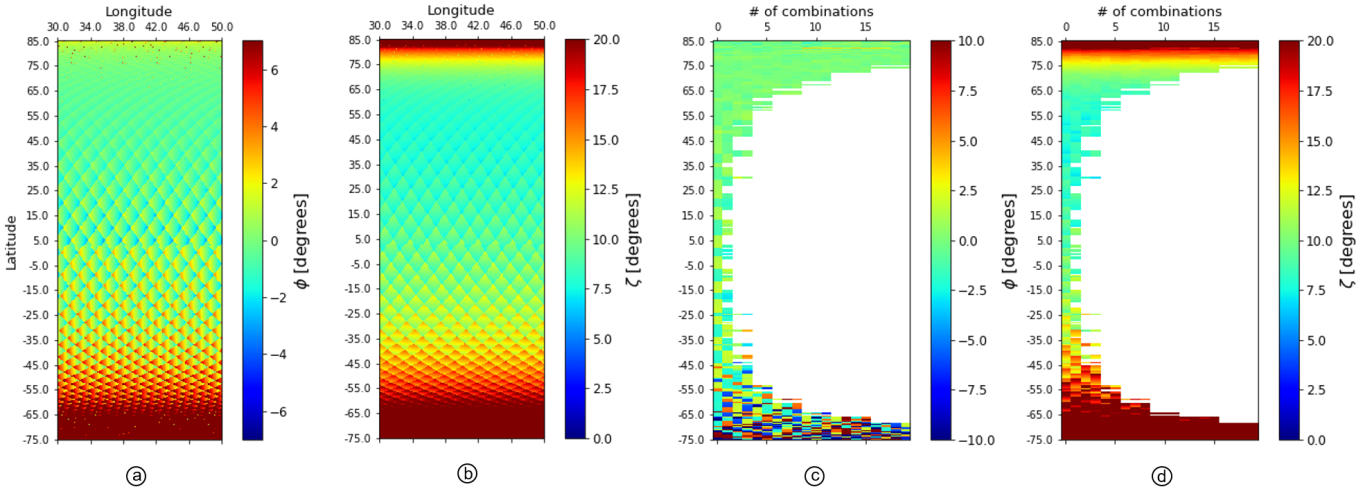

Fig. 7: Orientation of the null line for Sentinel-1, defined by ϕ and ζ, see Fig. 5. The checkered pattern is due to the S1 orbit pattern. (a): azimuth ϕ, (b): elevation ζ. Values are calculated by combining the ascending and descending observations that have a maximum azimuth of the ZDP, for each location on Earth, considering the maximum asymmetry between the two ZDP's. This demonstrates that $\phi \approx 0°$ for the Northern Hemisphere. (c) and (d), ϕ and ζ values for all possible combinations between overlapping ascending and descending acquisitions. Results computed using No-DRaMA [22].

the east-up (EU) plane[2]. Considering the null line in 3D, this line also has a projection onto the EU plane, which yields a line that we refer to as k, see Fig. 8. Line k has elevation angle

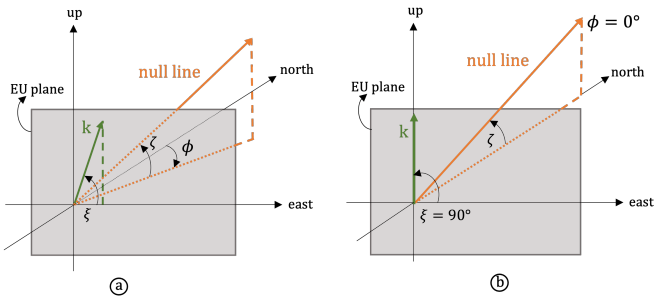

Fig. 8: The orientation of the null line n in the ENU reference frame is given by azimuth angle ϕ and elevation angle ζ. The projection of n onto the east-up (EU) plane is line k which has elevation angle ξ. In (a), $\phi \neq 0°$ and $\zeta \neq 0°$ and therefore k as a component in the east and up direction, i.e., $\xi \neq 90°$. In (b), $\phi = 0°$ and therefore $\xi = 90°$, k only has a component in the up direction, the component in the east direction is zero.

ξ, and as long as $\xi \neq 90°$ and $\xi \neq 0°$, k has both a component in the up and east direction, i.e., k contains infinitely many combinations of d_e and d_u. Consequently, it is not possible to give unbiased estimates for both d_e and d_n. If and only if $\phi = 0°$, line k has no component in the east direction and $\xi = 90°$. Only then, it is possible to give an unbiased estimate for d_e, albeit that d_u is still biased ($\zeta \neq 0$).

[2]Note that this is a *discretionary* projection, and not a *forced* projection, as introduced in Sec. II-B

The bias terms B_e and B_u are thus (i) dependent on the orientation of the null line n, and are (ii) scaled by the actual magnitude of the real-world displacements in the north direction, d_n, i.e.,

$$\begin{aligned} B_e &= \tan\phi \; d_n \\ B_u &= \tan\zeta \; d_n. \end{aligned} \tag{15}$$

This can also be seen in Fig. 9, where we visualized the relative errors for the estimated east and up displacements when we solve Eq. (13). The colored lines represent different proportions between the simulated north and east or up displacement component. It can indeed be seen that the more ϕ and ζ deviate from zero, the larger the relative errors for $\hat{d}_e$ and $\hat{d}_u$ respectively. The relative errors also scale with the magnitude of the north component.

C. The null line aligned (NLA) frame

Using the concept of the null line and its orientation in 3D space, we propose a null line aligned (NLA) coordinate system using the first axis in the local horizontal plane, the second axis aligned along the null-line, and the third one complementing the right-handed 3D Cartesian system. As stated above, projecting the two LoS observation vectors onto the plane orthogonal to the null line will, and solving for the two in-plane components, result in unbiased estimates for two displacement components. This unbiasedness make these result optimally suited for usage in mathematical or geophysical models.

V. Fallacy Categories in Current Practice

Comparing the conditions that should be fulfilled to estimate the unknown displacement parameters, see Sec. III, with the

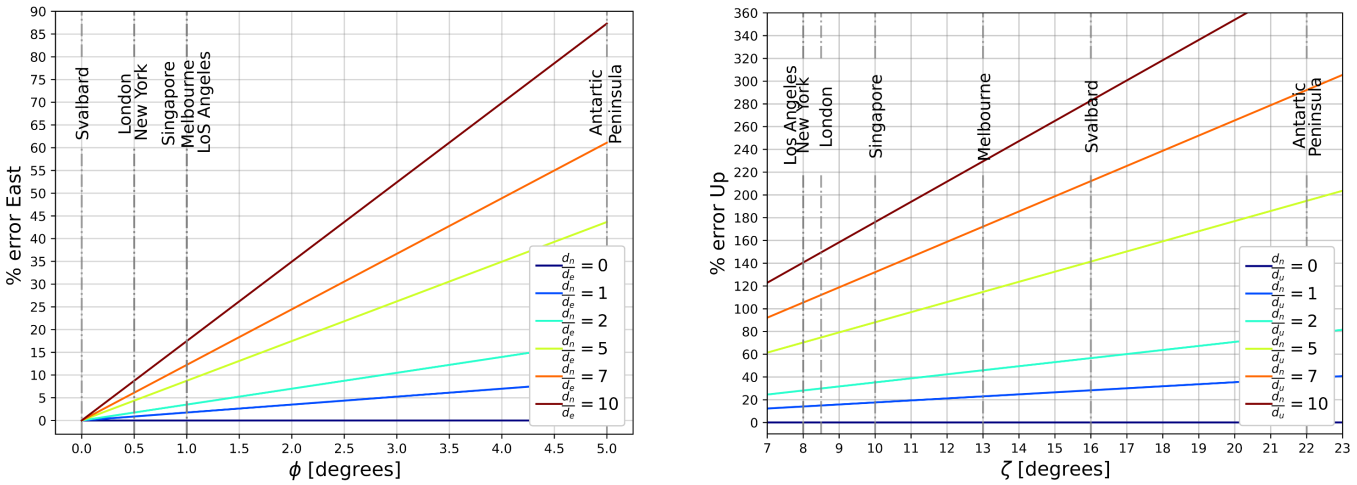

Fig. 9: Relative error for the estimated east and up displacement components when the north component is ignored and we solve Eq. (13). It can be seen that there is a relation between the orientation of the null line and the relative errors. The more ϕ and ζ deviate from zero, the larger the relative errors for $\hat{d}_e$ and $\hat{d}_u$ respectively. Moreover the size of the error depends on the size of the 'neglected' north displacement. We estimated the orientation of the null line (ϕ and ζ) for different locations in the world and we visualized these locations with the vertical gray lines. Note that for most cities, the relative error for the east component is not too large, since $\phi \approx 0°$. However, the error for the up component can be significant everywhere.

most common approaches we find in InSAR literature to address the underdeterminancy problem, we find that several approaches have either mathematical or semantic flaws. The impact of these flaws ranges from quantitative errors in the reported studies, mismatches in comparative studies with other geodetic techniques, to a lack of confidence in the technology by end-users. This creates an urgent need for more robust definitions and more transparent communication, to better serve the needs of both science and operational practice. We identify three distinct classes of geometric InSAR fallacies: attribution, projection, and decomposition.

A. Attribution error

Attribution errors occur when the line-of-sight observation is literally attributed to one displacement direction (usually the vertical), given only a single viewing geometry, without projection and without further justification. Obviously, this is erroneous, and results in a severe underestimation, i.e., bias, of vertical displacements of up to 40% (from $1/\cos\theta$ in Eq. (1)). While explicit attribution errors were more common in the early days of InSAR, ambiguous statements or colorbar labels can still be found in more recent literature ([34], [35], [36], [37], [38]) in which (the application of) a projection is not explicitly or uniquely described, feeding potential misinterpretation. For example, when only single-geometry LoS observations are available, using words such as 'subsidence', authors implicitly postulate vertical displacements, see e.g., [37], [39]. In these cases, explicitly stated assumptions would be vital for unambiguous interpretation.

B. Projection error

Projection errors occur, e.g., when LoS displacement estimates are '*projected onto the vertical*,' but are subsequently presented as '*vertical displacements*'. Obviously, the two would only be identical under the assumption that any non-vertical displacement component of the 3D displacement vector is zero. Since this assumption is in many cases incorrect, e.g., for landslides, but even for subsidence bowls, it leads to a biased estimate. Such a bias can have a significant impact combined with a small likelihood of being detected, which is the case in, e.g., [40], [41], [42], [43], [44]. In several studies, explicit assumptions on the non-existence of the horizontal component are not made at all, e.g., [45], [46], [47], [48]. Typically, projection errors are associated with indistinct verbs, such as 'converted', 'transformed', 'computed', 'calculated', or 'determined'. These all suggest that there is a unique relation between the LoS displacements and the vertical displacements, which is generically incorrect.

C. Decomposition error

The most frequently occurring geometric InSAR fallacy is a *decomposition error* which occurs when the existence of a null space is simply ignored, see Sec. IV. Typical examples of decomposition errors include explicit statements such as: (i) *"By combining an ascending and a descending time-series, it is possible to disentangle east-west horizontal deformation from vertical deformation."* [24], (ii) *"The combination of ascending and descending satellite passes allows the decomposition of the line of sight velocities into horizontal east-west and vertical components."* [31], (iii) *"Whenever two data sets of InSAR images are available, [...] the PS-InSAR results can be used successfully to estimate the vertical and east-west components of the local displacement fields."* [26], or (iv) *"Using data from both ascending and descending orbits, it is possible to determine the vertical displacement and one component of horizontal displacement."* [27]. These

statements have in common that they suggest that it is possible to unambiguously and unbiasedly 'disentangle', 'estimate', 'determine', 'compute', or 'reconstruct' two displacements components, usually the vertical and east component, with two LoS observations. However, as discussed in Sec. IV-B, with these viewing geometries this will always result in biased estimates, except for the NLA coordinate system proposed in Sec. IV-C. Note that the term 'east-west' motion should be avoided since the term is ambiguous, as there is no sign convention. It should be replaced by 'east' motion, where east would be positive and west motion would be negative.

Some authors also try to decompose the observations into the plane spanned by the up direction and the azimuth look direction of one of the satellites, see [32], [45]. This approach is also incorrect (i.e., biased) since this plane is never equal to the plane orthogonal to the null line.

A second variant of a decomposition error is a consequence of incorrect underlying assumptions. For example, it is often assumed that due to the *lack of sensitivity* for the north-component, d_n can be removed from the inverse problem altogether, e.g., [23], [24], [25], [26], [27], [28], [29], [30], [31], [32], [33], [49]. This assumption would only be valid if the orientation of the null line $n(\phi, \zeta)$ is both in the north direction as well as horizontal, i.e., $(\phi, \zeta) = (0, 0)$, which is never the case, see Fig. 7. Some examples of erroneous assumptions include *(i) "Assuming that the orbital path of the satellite is approximately parallel to the meridian, the LOS sensitivity to motion in the N-S direction is negligible, hence the equation can be rewritten [...] to estimate vertical and E–W motion."* [30], *(ii) "The north-south component can be neglected due to the low sensitivity of SAR sensors along that direction."* [33], or *(iii) "The sensitivity to a target motion along the north-south direction is usually quite low."* [26]. Simply removing d_n from Eq. (4) under the assumption of the low sensitivity for that component, without any knowledge of (or explicit statements on) the expected magnitude of the north-component, is not permissible: as long as the real-world displacement component into the north-direction is large enough, i.e., larger than the noise level of the projected LoS observations, it can still be discriminated from the observations.

The third and final variant of a decomposition error occurs when it is argued that *due to* the insensitivity to displacements into the north direction, one has to conclude that $d_n = 0$.[3] Obviously, this assumption refers to the actual size of the physical signal, i.e., the unknown parameter, which is evidently *not* correlated to the sensitivity of a particular radar instrument. Example quotes are *(i)"The north component is insensitive [...] consequently, we add the additional constraint that the north-south motion is assumed to be zero. In this way, we calculate the velocity in east-west and up-down direction."*[31], *(ii) "Sentinel-1 data are insensitive to north-south displacements direction [...] Therefore, we assumed that $d_n = 0$, and this allowed us to find the other two components of the deformation vector."* [28], and *(iii) "It is also assumed that horizontal velocities are mainly due to east–west motion, owing to InSAR low sensitivity to the north component."* [32].

In conclusion, either the implicit assumption that with two observation geometries we can estimate any arbitrary two directions in 3D space (including the fashionable EU decomposition), or deliberately ignoring d_n, or simply assuming that d_n is known, all lead to an erroneous (i.e., biased) decomposition.

VI. Recommendations for InSAR product generation and interpretation

While the underdetermined nature of the problem cannot be formally solved, we propose recommendations for InSAR product generation and interpretation. First, we discuss two options for performing a displacement vector *decomposition* given two viewing geometries. Then, we evaluate the options for displacement vector *projection* onto a 1D direction and a 2D plane.

A. Recommendations for vector decomposition

A decomposition of two LoS observations is feasible when the two LoS observations are STCI. Yet, as this is practically impossible, we need to define a RUM, and perform a datum connection, see Section III. Given the model of observation equations of Eqs. (4) and (5) with only two observation geometries, the only way to reduce the rank deficiency is to reduce the parameter space from three to two unknown parameters. This goal can be achieved in two ways.

The first 'physical' option is to change the orientation of the Cartesian reference frame in combination with a priori physical information: the *strap-down system* [50]. For example, for many physical phenomena gravity is the driving force for displacements, which allows us to define a two-dimensional vertical plane in which the displacement vector is expected to be situated. Examples include landslides and glaciers, where this plane is spanned by the vector normal to the slope and the gravity vector [51], [52], [53], [54], or for line infrastructure where it may be assumed that no displacements occur in its longitudinal direction [55], [56]. Both require a known rotation of the Cartesian frame such that one direction can be assumed to be displacement-free. Consequently, any frame misalignment will result in biased estimates, see Section IV.

A second 'geometric' option is to take advantage of the orientation of the null space, by choosing a *null line aligned* (NLA) Cartesian coordinate system, see Section IV-C. This yields a plane orthogonal to the null line, and the (forced) orthogonal projection of a displacement vector onto that plane will not influence (bias) the two in-plane components. Thus, these in-plane components can be uniquely and unbiasedly estimated. This option is particularly recommended when the InSAR results are used as input in a physical or mathematical model, since their unbiased nature will not compromise the output of that model.

For both the 'physical' and the 'geometrical' option, we recommend to explicitly mention the orientation of the null line with the InSAR product since it comprises information on the direction in which displacements cannot be observed.

[3]Note that the $d_n = 0$ assumption is a specific case of the more generic assumption that $d_n = c$, i.e., d_n is known.

Frequently used alternative options are not recommended. Theoretically, when it would be known from physics that a displacement component is zero in a cardinal compass direction, i.e., a northbound component equal to zero ($d_n = 0$), the parameter space has dimension two, and the remaining parameters may be uniquely estimated. However, while this physics-based rank-reduction may not be impossible, e.g. considering perfectly east-west oriented faults [6], it is a solution that is in a generic sense physically unrealistic and often unsubstantiated, since dynamic processes on earth typically do not have a preference for a cardinal compass direction.

Likewise, we do not recommend the widely advocated and applied decomposition in the EU-plane, as this introduces biases, is prone to misinterpretation, and suggests an estimation possibility that is non-existent.

B. Recommendations for vector projection

When there is no deformation direction in which displacements are known to be zero, or when it is inconvenient to decompose the two LoS observations in the plane orthogonal to the null line, it will not be possible to *decompose* the LoS observations. Yet, a *projection* is an operation that that is admissible and can always be performed without exceptions or assumptions. Clearly, a projection product is different from *estimating* the unknown parameters. Moreover, 'projection-onto' (P/O) products are *discretionary* projections, and it is up to the end-user to decide on whether such a projection contains intelligible information. We distinguish *projection* onto a 1D direction from a single viewing geometry, and onto a 2D plane from dual viewing geometries.

1) Projecting one LoS observation onto one direction: With only one LoS observation available, it is possible to project that observation onto any particular direction. For example, often d_{LoS} is projected onto the vertical direction using

$$d_{\text{up}}^{\text{P/O}} = P_{\text{up, LoS}^\perp}\, d_{\text{LoS}} = (\cos\theta)^{-1} d_{\text{LoS}}, \tag{16}$$

where $P_{\text{up, LoS}^\perp}$ is the projector, and $d_{\text{up}}^{\text{P/O}}$ is the projection of d_{LoS} onto the up direction. Note that in general $d_{\text{up}}^{\text{P/O}} \neq d_{\text{up}}$. The operation is an *oblique* projection of the LoS observations onto the vertical axis, along a plane orthogonal to the LoS unit vector. In contrast, when the LoS observations would be projected *orthogonally* onto the vertical, i.e., along a plane orthogonal to the 'up' unit vector, that would result in

$$d_{\text{up}}^{\text{P/O}^\perp} = P_{\text{up, up}^\perp}\, d_{\text{LoS}} = \underbrace{\begin{bmatrix} 0 & 0 & 0 \\ 0 & 0 & 0 \\ 0 & 0 & 1 \end{bmatrix}}_{P} \mathbf{u}_{\text{LoS}} d_{\text{LoS}} = \cos\theta\; d_{\text{LoS}}, \tag{17}$$

which differs from Eq. (16). Thus, both $P_{\text{up, LoS}^\perp}$ and $P_{\text{up, up}^\perp}$ are allowable discretionary projectors, but with a completely different result. Note that the oblique projection in Eq. (16) may be counter-intuitive, as the result ($d_{\text{up}}^{\text{P/O}}$) can be greater than the vector that is projected (d_{LoS}). For the orthogonal projection, the absolute value of the result will always be smaller than the vector that is projected.

The main recommendation is therefore to (i) explicitly mention the use of a *projection-onto* product, and (ii) explicitly distinguish an oblique from an orthogonal projection. This is required both in text as well as in cartographic symbols and, e.g., colorbar annotations. Furthermore, we recommend to present the orientation of the null plane, which is described by the LoS vector that is orthogonal to this plane, since it is the plane where no displacements can be observed.

2) Projecting two LoS observations onto a plane: When two LoS observations are available, the observations can be projected onto any arbitrary plane, e.g., orthogonal onto the EU-plane spanned by the east and the vertical axis, and estimates $\hat{d}_e^{\text{P/O}^\perp}$ and $\hat{d}_u^{\text{P/O}^\perp}$ in that plane can be found. When a LoS displacement vector is projected onto the plane spanned by the east and up axis, i.e., the EU plane, we have

$$d_{\text{EU}}^{\text{P/O}^\perp} = \underbrace{\begin{bmatrix} 1 & 0 & 0 \\ 0 & 0 & 0 \\ 0 & 0 & 1 \end{bmatrix}}_{P} \mathbf{u}_{\text{LoS}} d_{\text{LoS}}, \tag{18}$$

where $d_{\text{EU}}^{\text{P/O}}$ is the projection of d_{LoS} onto the EU plane. When this projection is performed for the two LoS observations it is possible to transform the observations into east and up components with Eq. (13). However, it should be stressed that the results of the discretionary projection, $(d_e^{\text{P/O}}, d_u^{\text{P/O}})$, are not the same as the unknown displacement components (d_e, d_u).

C. Presenting LoS observations unaltered

The last option for handling the underdetermined problem we show here, is presenting the LoS observations unaltered as the final product. This is obviously correct, as it does not attempt to do any projection, attribution, or decomposition, as in [23], [57], [58], [59]. The drawback of the LoS product is that it is typically more difficult to interpret, especially for non-experts: as potential vertical and horizontal displacement components are projected onto the LoS and superposed, what happens in the real world remains obscured. Yet, this is the preferred option when the InSAR results are used as input in a physical or mathematical model, since their unbiased nature will not compromise the output of that model.

VII. Conclusions

In many InSAR-based studies and products, the restrictions of the typical satellite InSAR geometry are often not well represented in results, both textual and in maps and graphs. Three classes of fallacies have been identified, related to attribution, projection, and decomposition. Decomposition fallacies often suggest the possibility to unbiasedly estimate two directional components from two viewing geometries, i.e., east and up. Using the orbital and viewing characteristics, linear algebra shows that this is generically not correct, leading to biased estimation of the east and particularly the up components. The impact of this bias depends on the situation at hand, and should not by trivialized.

Introducing the concept of the null line, we suggest a possibility for the unbiased estimation of two orthogonal

components, using a *null line aligned* (NLA) Cartesian coordinate system. Use of this coordinate system is particularly recommended when the InSAR results are to be used as displacement input in mathematical models. Alternatively, we recommend the use of discretionary projections, as long as they are explicitly mentioned. In this context it is important to stress the difference between, e.g., a vertical displacement, and a displacement projected onto the vertical, as well as the difference between an oblique and an orthogonal projection. Proper mathematical symbols are essential. A third option is the use of a *strap-down* system, where the rank deficiency is resolved by assuming a locally varying coordinate system, where the displacement in one of the cardinal directions can be assumed to be void.

When a decomposition is required, i.e., the estimation of orthogonal displacement components, we state the conditions under which this is allowable. Strictly, all LoS observations need to be spatio-temporally coinciding and independent (STCI). As this is practically impossible, we need to define regions of uniform motion (RUMs), perform a datum connection between the independent viewing geometries, and guarantee a full-rank system with sufficient angular diversity.

Given the importance of the null line, we compute its orientation for all possible latitudes, and determine the maximum angular diversity per latitude given all available orbits of a given sensor. The corresponding code, No-Drama, is made available via gitlab [22], and may be used to compute the null line orientation for any particular location on Earth. We recommend to state the null line (or null-space) orientation explicitly with any InSAR result, as it is a fundamental metric required for a proper interpretation.

ACKNOWLEDGMENT

REFERENCES

[1] R. F. Hanssen, *Radar interferometry: data interpretation and error analysis*. Springer Science & Business Media, 2001, vol. 2.

[2] D. Massonnet, M. Rossi, C. Carmona, F. Adagna, G. Peltzer, K. Feigl, and T. Rabaute, "The displacement field of the Landers earthquake mapped by radar interferometry," *Nature*, vol. 364, no. 8, pp. 138–142, Jul.-8 1993.

[3] H. A. Zebker, P. A. Rosen, R. M. Goldstein, A. Gabriel, and C. L. Werner, "On the derivation of coseismic displacement fields using differential radar interferometry: The Landers earthquake," *Journal of Geophysical Research*, vol. 99, no. B10, pp. 19 617–19 634, Oct.-10 1994.

[4] D. Massonnet and K. L. Feigl, "Satellite radar interferometric map of the coseismic deformation field of the M = 6.1 Eureka Valley, California earthquake of May 17, 1993," *Geophysical Research Letters*, vol. 22, no. 12, pp. 1541–1544, 1995.

[5] Y. Fialko, M. Simons, and D. Agnew, "The complete (3-D) surface displacement field in the epicentral area of the 1999 mw 7.1 Hector Mine earthquake, California, from space geodetic observations," *Geophysical Research Letters*, vol. 28, no. 16, p. 3063, 2001.

[6] T. J. Wright, B. E. Parsons, and Z. Lu, "Towards mapping surface deformation in three dimensions using InSAR," *Geophysical Research Letters*, vol. 31, p. 5 pp., 2004.

[7] J. Hu, Z. Li, X. Ding, J. Zhu, L. Zhang, and Q. Sun, "Resolving three-dimensional surface displacements from InSAR measurements: A review," *Earth-Science Reviews*, vol. 133, pp. 1–17, 2014.

[8] T. Fuhrmann and M. C. Garthwaite, "Resolving three-dimensional surface motion with InSAR: Constraints from multi-geometry data fusion," *Remote Sensing*, vol. 11, no. 3, p. 241, 2019.

[9] G. Strang, *Linear algebra and its applications*, 3rd ed. Fort Worth: Harcourt Brace Jovanovich College Publishers, 1988.

[10] F. Rocca, "3d motion recovery with multi-angle and/or left right interferometry," in *Proceedings of the third International Workshop on ERS SAR*, 2003.

[11] European Space Agency. (2021) Sentinel 1 SAR Acquisition Modes. [Online]. Available: https://sentinels.copernicus.eu/web/sentinel/user-guides/sentinel-1-sar/acquisition-modes/interferometric-wide-swath

[12] P. Lopez-Dekker and A. Theodosiou. (2022) DRaMA software. [Online]. Available: https://gitlab.tudelft.nl/drama/drama

[13] A. Tarantola, *Inverse Problems Theory*. New York: Elsevier, 1987.

[14] P. J. G. Teunissen, *Adjustment theory*. VSSD Delft, 2003.

[15] P. Dheenathayalan, D. Small, A. Schubert, and R. F. Hanssen, "High-precision positioning of radar scatterers," *Journal of Geodesy*, vol. 90, no. 5, pp. 403–422, 2016.

[16] M. Yang, P. López-Dekker, P. Dheenathayalan, F. Biljecki, M. Liao, and R. F. Hanssen, "Linking persistent scatterers to the built environment using ray tracing on urban models," *IEEE Transactions on Geoscience and Remote Sensing*, vol. 57, no. 8, pp. 5764–5776, 2019.

[17] X. X. Zhu, S. Montazeri, C. Gisinger, R. Hanssen, and R. Bamler, "Geodetic TomoSAR—fusion of SAR imaging geodesy and TomoSAR for 3D absolute scatterer positioning," in *2014 IEEE Geoscience and Remote Sensing Symposium*. IEEE, 2014, pp. 1317–1320.

[18] X. X. Zhu, S. Montazeri, C. Gisinger, R. F. Hanssen, and R. Bamler, "Geodetic SAR tomography," *IEEE Transactions on Geoscience and Remote Sensing*, vol. 54, no. 1, pp. 18–35, 2015.

[19] R. F. Hanssen, "A radar retroreflector device and a method of preparing a radar retroflector device," patent, 12 27, 2018.

[20] V. B. H. Ketelaar, *Monitoring surface deformation induced by hydrocarbon production using satellite radar interferometry*. Springer, Sep. 2008.

[21] F. Rocca, "3D motion recovery with multi-angle and/or left right interferometry," in *Proceedings of the third International Workshop on ERS SAR*. Citeseer, 2003.

[22] W. Brouwer and R. Hanssen, *No-DRaMA software*, 2022. Retrieved on: July 14, 2022, from https://gitlab.tudelft.nl/drama/drama/-/tree/acquisitionsv0. [Online]. Available: https://gitlab.tudelft.nl/drama/drama/-/tree/acquisitionsv0

[23] B. V. Yazici and E. Tunc Gormus, "Investigating persistent scatterer InSAR (PSInSAR) technique efficiency for landslides mapping: a case study in Artvin dam area, in Turkey," *Geocarto International*, pp. 1–19, 2020.

[24] H. Klemm, I. Quseimi, F. Novali, A. Ferretti, and A. Tamburini, "Monitoring horizontal and vertical surface deformation over a hydrocarbon reservoir by PSInSAR," *First break*, vol. 28, no. 5, 2010.

[25] A. Rucci, D. Vasco, and F. Novali, "Monitoring the geologic storage of carbon dioxide using multicomponent SAR interferometry," *Geophysical Journal International*, vol. 193, no. 1, pp. 197–208, 2013.

[26] C. Janna, N. Castelletto, M. Ferronato, G. Gambolati, and P. Teatini, "A geomechanical transversely isotropic model of the Po river basin using PSInSAR derived horizontal displacement," *International Journal of Rock Mechanics and Mining Sciences*, vol. 51, pp. 105–118, 2012.

[27] S. Yun, P. Segall, and H. Zebker, "Constraints on magma chamber geometry at Sierra Negra volcano, Galápagos Islands, based on InSAR observations," *Journal of Volcanology and geothermal research*, vol. 150, no. 1-3, pp. 232–243, 2006.

[28] K. Pawluszek-Filipiak and A. Borkowski, "Integration of DInSAR and SBAS techniques to determine mining-related deformations using Sentinel-1 data: The case study of Rydułtowy mine in Poland," *Remote Sensing*, vol. 12, no. 2, p. 242, 2020.

[29] P. Teatini, N. Castelletto, M. Ferronato, G. Gambolati, C. Janna, E. Cairo, D. Marzorati, D. Colombo, A. Ferretti, A. Bagliani *et al.*, "Geomechanical response to seasonal gas storage in depleted reservoirs: A case study in the Po river basin, Italy," *Journal of Geophysical Research: Earth Surface*, vol. 116, no. F2, 2011.

[30] A. Tamburini, M. Bianchi, C. Giannico, and F. Novali, "Retrieving surface deformation by PSInSAR™ technology: A powerful tool in reservoir monitoring," *International Journal of Greenhouse Gas Control*, vol. 4, no. 6, pp. 928–937, 2010.

[31] D. H. T. Minh, N. Yen-Nhi, T. T. Lê, T. C. Le, H. S. Bui, Q. V. Vuong, and T. Le Toan, "Quantifying horizontal and vertical movements in Ho Chi Minh city by Sentinel-1 radar interferometry," 2021.

[32] S. Alatza, I. Papoutsis, D. Paradissis, C. Kontoes, G. A. Papadopoulos, and C. Raptakis, "InSAR time-series analysis for monitoring ground displacement trends in the western Hellenic Arc: The Kythira Island, Greece," *Geosciences*, vol. 10, no. 8, p. 293, 2020.

[33] M. Imamoglu, F. Kahraman, Z. Cakir, and F. B. Sanli, "Ground deformation analysis of Bolvadin (w. Turkey) by means of multi-temporal

InSAR techniques and Sentinel-1 data," *Remote Sensing*, vol. 11, no. 9, p. 1069, 2019.
[34] L. Zhou, J. Guo, J. Hu, J. Li, Y. Xu, Y. Pan, and M. Shi, "Wuhan surface subsidence analysis in 2015–2016 based on sentinel-1a data by SBAS-InSAR," *Remote Sensing*, vol. 9, no. 10, p. 982, 2017.
[35] P. Teatini, L. Tosi, T. Strozzi, L. Carbognin, U. Wegmüller, and F. Rizzetto, "Mapping regional land displacements in the Venice coastland by an integrated monitoring system," *Remote Sensing of Environment*, vol. 98, no. 4, pp. 403–413, 2005.
[36] S. Stramondo, F. Bozzano, F. Marra, U. Wegmuller, F. Cinti, M. Moro, and M. Saroli, "Subsidence induced by urbanisation in the city of Rome detected by advanced InSAR technique and geotechnical investigations," *Remote Sensing of Environment*, vol. 112, no. 6, pp. 3160–3172, 2008.
[37] L. Solari, A. Ciampalini, F. Raspini, S. Bianchini, and S. Moretti, "PSInSAR analysis in the Pisa urban area (Italy): a case study of subsidence related to stratigraphical factors and urbanization," *Remote Sensing*, vol. 8, no. 2, p. 120, 2016.
[38] M. Zheng, K. Deng, H. Fan, and S. Du, "Monitoring and analysis of surface deformation in mining area based on InSAR and GRACE," *Remote Sensing*, vol. 10, no. 9, p. 1392, 2018.
[39] N. Svigkas, C. Loupasakis, P. Tsangaratos, I. Papoutsis, A. Kiratzi, and C. H. Kontoes, "A deformation study of Anthemountas graben (northern Greece) based on in situ data and new InSAR results," *Arabian Journal of Geosciences*, vol. 13, no. 13, pp. 1–13, 2020.
[40] A. H.-M. Ng, H. Wang, Y. Dai, C. Pagli, W. Chen, L. Ge, Z. Du, and K. Zhang, "InSAR reveals land deformation at Guangzhou and Foshan, China between 2011 and 2017 with COSMO-SkyMed data," *Remote Sensing*, vol. 10, no. 6, p. 813, 2018.
[41] M. Haghshenas Haghighi and M. Motagh, "Sentinel-1 InSAR over Germany: Large-scale interferometry, atmospheric effects, and ground deformation mapping," *ZfV: Zeitschrift für Geodäsie, Geoinformation und Landmanagement*, vol. 2017, no. 4, pp. 245–256, 2017.
[42] R. Bonì, F. Cigna, S. Bricker, C. Meisina, and H. McCormack, "Characterisation of hydraulic head changes and aquifer properties in the london basin using persistent scatterer interferometry ground motion data," *Journal of Hydrology*, vol. 540, pp. 835–849, 2016.
[43] W. Tang, P. Yuan, M. Liao, and T. Balz, "Investigation of ground deformation in Taiyuan Basin, China from 2003 to 2010, with atmosphere-corrected time series InSAR," *Remote Sensing*, vol. 10, no. 9, p. 1499, 2018.
[44] R. N. Nof, G. Baer, A. Ziv, E. Raz, S. Atzori, and S. Salvi, "Sinkhole precursors along the Dead Sea, Israel, revealed by SAR interferometry," *Geology*, vol. 41, no. 9, pp. 1019–1022, 2013.
[45] S. Alatza, I. Papoutsis, D. Paradissis, C. Kontoes, and G. A. Papadopoulos, "Multi-temporal insar analysis for monitoring ground deformation in amorgos island, greece," *Sensors*, vol. 20, no. 2, p. 338, 2020.
[46] N. Short, A.-M. LeBlanc, W. Sladen, G. Oldenborger, V. Mathon-Dufour, and B. Brisco, "RADARSAT-2 D-InSAR for ground displacement in permafrost terrain, validation from Iqaluit Airport, Baffin Island, Canada," *Remote Sensing of Environment*, vol. 141, pp. 40–51, 2014.
[47] D. Raucoules, C. Maisons, C. Carnec, S. Le Mouelic, C. King, and S. Hosford, "Monitoring of slow ground deformation by ERS radar interferometry on the Vauvert salt mine (France): Comparison with ground-based measurement," *Remote sensing of environment*, vol. 88, no. 4, pp. 468–478, 2003.
[48] H. Sun, Q. Zhang, C. Zhao, C. Yang, Q. Sun, and W. Chen, "Monitoring land subsidence in the southern part of the lower Liaohe plain, China with a multi-track PS-InSAR technique," *Remote sensing of environment*, vol. 188, pp. 73–84, 2017.
[49] A. Pepe and F. Calò, "A review of interferometric synthetic aperture radar (InSAR) multi-track approaches for the retrieval of Earth's surface displacements," *Applied Sciences*, vol. 7, no. 12, p. 1264, 2017.
[50] W. Brouwer and R. Hanssen, "Estimating 3 dimensional displacements with InSAR: the strap-down solution," *In preparation*, vol. xx, p. xxxx, 2022.
[51] J. J. Mohr, "Repeat track SAR interferometry. an investigation of its utility for studies of glacier dynamics," Ph.D. dissertation, Technical University of Denmark, Copenhagen, May 1997.
[52] L. Cascini, G. Fornaro, and D. Peduto, "Advanced low-and full-resolution DInSAR map generation for slow-moving landslide analysis at different scales," *Engineering Geology*, vol. 112, no. 1-4, pp. 29–42, 2010.
[53] V. Greif and J. Vlcko, "Monitoring of post-failure landslide deformation by the PS-InSAR technique at Lubietova in central Slovakia," *Environmental Earth Sciences*, vol. 66, no. 6, pp. 1585–1595, 2012.
[54] A. L. van Natijne, T. A. Bogaard, F. J. van Leijen, R. F. Hanssen, and R. C. Lindenbergh, "World-wide InSAR sensitivity index for landslide deformation tracking," *Int. J. Appl. Earth Obs. and Geoinf.*, vol. accepted for publication, no. in press, pp. 1–10, 2022.
[55] I. E. Özer, F. J. van Leijen, S. N. Jonkman, and R. F. Hanssen, "Applicability of satellite radar imaging to monitor the conditions of levees," *Journal of Flood Risk Management*, vol. 12, no. S2, p. e12509, 2019.
[56] L. Chang, R. P. Dollevoet, and R. F. Hanssen, "Monitoring line-infrastructure with multisensor sar interferometry: products and performance assessment metrics," *IEEE journal of selected topics in applied earth observations and remote sensing*, vol. 11, no. 5, pp. 1593–1605, 2018.
[57] N. Fatholahi, M. Akhoondzadeh, and A. Bahroudi, "An investigation of surface deformation over oilfield in southwest Iran (2003–2010) using InSAR and physical modelling," *International Journal of Remote Sensing*, vol. 41, no. 14, pp. 5355–5370, 2020.
[58] R. Guo, L. Sumin, Y. Chen, X. Li, and L. Yuan, "Identification and monitoring landslides in longitudinal range-gorge region with InSAR fusion integrated visibility analysis," *Landslides*, pp. 1–18, 2020.
[59] L. Wang, K. Deng, and M. Zheng, "Research on ground deformation monitoring method in mining areas using the probability integral model fusion D-InSAR, sub-band InSAR and offset-tracking," *International Journal of Applied Earth Observation and Geoinformation*, vol. 85, p. 101981, 2020.

Wietske Brouwer received the BSc degree and MSc degrees in Civil Engineering from Delft University of Technology in 2018 and 2021, respectively. She is currently pursuing her PhD degree at TU Delft, working on mathematical aspects of satellite radar interferometry.

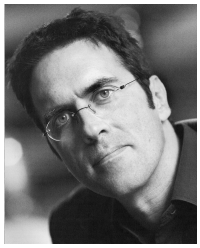

Ramon F. Hanssen (M'04-SM'15) received the M.Sc. degree in Geodetic Engineering and the Ph.D. degree (cum laude) from Delft University of Technology, The Netherlands, in 1993 and 2001, respectively.

He was with the International Institute for Aerospace Survey and Earth Science (ITC), Stuttgart University, Stuttgart, Germany; the German Aerospace Center (DLR), Weßling, Germany; Stanford University, Stanford, CA, USA, as a Fulbright Fellow; and the Scripps Institution of Oceanography, University of California at San Diego, La Jolla, CA, USA, involved in microwave remote sensing, radar interferometry, signal processing, and geophysical application development. Since 2008, he has been an Antoni van Leeuwenhoek Professor in earth observation with the Delft University of Technology, where he has been leading the research group on mathematical geodesy and positioning since 2009. He has authored a textbook on radar interferometry.